



Schweizerischer Erdbebendienst  
Service Sismologique Suisse  
Servizio Sismico Svizzero  
Servizi da Terratrembels Svizzer



Eidgenössische Technische Hochschule Zürich  
Swiss Federal Institute of Technology Zurich

---

# **Obervaz - Muldain (SVAM)**

## **SITE CHARACTERIZATION REPORT**

**Clotaire MICHEL, Jan BURJANEK, Valerio POGGI,  
Carlo CAUZZI, Daniel ROTEN, Donat FÄH**

---



Sonneggstrasse 5 CH-8092 Zürich Switzerland; E-mail: [clotaire.michel@sed.ethz.ch](mailto:clotaire.michel@sed.ethz.ch)

Last modified : November 5, 2013

## Abstract

Ambient vibration array measurements were performed in Obervaz-Muldain, close to station SVAM that is part of the Swiss Strong Motion network (SSMNet). It is supposed to be located on a slowly moving unstable rock slope. H/V processing of the array data leads to a stable peak value of 4 Hz, but with low amplitudes. The velocity profiles below station SVAM exhibit a 5 m depth layer of sand (200 m/s) and a layer of weathered rock (700 m/s) down to the bedrock at 45 m depth with a velocity around 2700 m/s (not really constrained).  $V_{s,30}$  is found to be 486 m/s. The site can be classified as type B in the Eurocode 8 and type E in the Swiss Code SIA261. Other geological and geophysical data should be collected to learn more about this mass movement, the distribution of the sand layer and the weathering and fracturing of the rock. Recordings at the station will also allow to update the assumptions made here.

<i>CONTENTS</i>	3
<b>Contents</b>	
<b>1 Introduction</b>	<b>4</b>
<b>2 Experiment description</b>	<b>5</b>
2.1 Ambient Vibrations . . . . .	5
2.2 Equipment . . . . .	5
2.3 Geometry of the arrays . . . . .	5
2.4 Positioning of the stations . . . . .	6
<b>3 Data quality</b>	<b>7</b>
3.1 Usable data . . . . .	7
3.2 Data processing . . . . .	7
<b>4 H/V processing</b>	<b>8</b>
4.1 Processing method and parameters . . . . .	8
4.2 Results . . . . .	8
<b>5 Array processing</b>	<b>12</b>
5.1 Processing methods and parameters . . . . .	12
5.2 Obtained dispersion curves . . . . .	12
<b>6 Inversion and interpretation</b>	<b>16</b>
6.1 Inversion . . . . .	16
6.2 Travel time average velocities and ground type . . . . .	20
6.3 SH transfer function and quarter-wavelength velocity . . . . .	20
<b>7 Conclusions</b>	<b>23</b>
<b>References</b>	<b>25</b>

# 1 Introduction

The station SVAM (Vaz-Muldain) is part of the Swiss Strong Motion Network (SSMNet) in the Graubünden. This station, one of the first SSMNet station, installed in 1991, was renewed in the frame of the SSMNet Renewal project in 2011, moving the sensor outside the Muldain transformer house (2 m). This project includes also the site characterization. The passive array measurement technique has been selected as a standard tool to investigate these sites. The measurement campaign was done on 17<sup>th</sup> August 2010 in Obervaz-Muldain (Fig. 1), with the central station 50 m far from the station SVAM, in order to characterize the underground structure. The station is located on a large moving rock-slope that moves with velocities of half a centimeter every year (according to the local authorities). According to our knowledge, no global study was undertaken up to now to map this slope. This report presents the measurement setup, the results of the H/V analysis especially the fundamental frequency and of the array processing of the surface waves (dispersion curves). Then, an inversion of these results into velocity profiles is performed.

Canton	City	Location	Station code	Site type	Slope
Graubünden	Obervaz	Muldain	SVAM	Moving slope	$> 15^\circ$

Table 1: Main characteristics of the study-site.



Figure 1: Picture of the site.

## 2 Experiment description

### 2.1 Ambient Vibrations

The ground surface is permanently subjected to ambient vibrations due to:

- natural sources (ocean and large-scale atmospheric phenomena) below 1 Hz,
- local meteorological conditions (wind and rain) at frequencies around 1 Hz ,
- human activities (industrial machines, traffic...) at frequencies above 1 Hz [Bonney-Claudet et al., 2006].

The objective of the measurements is to record these ambient vibrations and to use their propagation properties to infer the underground structure. First, the polarization of the recorded waves (H/V ratio) are used to derive the resonance frequencies of the ground layers. Second, the arrival time delays between stations is used to derive the velocity of surface waves at different frequencies (dispersion). The information (H/V, dispersion curves) is then used to derive the properties of the soil layers using an inversion process.

### 2.2 Equipment

For these measurements 12 Quanterra Q330 dataloggers named NR01 to NR12 and 14 Lennartz 3C 5 s seismometers were available (see Tab. 2). Each datalogger can record on 2 ports A (channels EH1, EH2, EH3 for Z, N, E directions) and B (channels EH4, EH5, EH6 for Z, N, E directions). The time synchronization was ensured by GPS. The sensor are placed on a metal tripod in a 20 cm hole, when possible, for a better coupling with the ground.

<b>Digitizer</b>	<b>Model</b>	<b>Number</b>	<b>Resolution</b>
	Quanterra Q330	12	24 bits
<b>Sensor type</b>	<b>Model</b>	<b>Number</b>	<b>Cut-off frequency</b>
Velocimeter	Lennartz 3C	14	0.2 Hz

Table 2: Equipment used.

### 2.3 Geometry of the arrays

Two array configurations were used, for a total of 4 rings of 10, 25, 50 and 100 m radius around a central station. The first configuration includes the 3 inner rings with 14 sensors; the second configuration includes the 2 outer rings with 11 sensors. The minimum inter-station distance and the aperture are therefore 10 and 100 m and 50 and 200 m, respectively. The experimental setup is displayed in Fig. 2. The final usable datasets are detailed in Section 3.2.



Figure 2: Geometry of the arrays.

## 2.4 Positioning of the stations

The sensor coordinates were measured using a differential GPS device (Leica Viva GS10), including only a rover station and using the Real Time Kinematic technique provided by Swisstopo. It allows an absolute positioning with an accuracy better than 5 cm on the Swissgrid.

### 3 Data quality

#### 3.1 Usable data

The largest time windows were extracted, for which all the sensors of the array were in position and the GPS synchronization was ensured. The characteristics of the datasets are detailed in Tab. 3.

Station NR04 (points VAM201 and VAM403) did not write data on the Baler that was not well configured. Moreover, the vertical component at point VAM102 (station NR07 port B) failed due to the extension cable.

#### 3.2 Data processing

The data were first converted to SAC format including in the header the coordinates of the point (CH1903 system), the recording component and a name related to the position. The name is made of 3 letters characterizing the location (VAM here), 1 digit for the ring and 2 more digits for the number in the ring. The response of the sensor was not corrected and the values (in counts) were not converted to m/s.

<b>Dataset</b>	<b>Starting Date</b>	<b>Time</b>	<b>Length</b>	$F_s$	<b>Min. inter-distance</b>	<b>Aperture</b>	<b># of points</b>
1	2010/08/17	09:21	137 min	200 Hz	10 m	100 m	12
2	2010/08/17	12:33	87 min	200 Hz	50 m	200 m	10

Table 3: Usable datasets.

## 4 H/V processing

### 4.1 Processing method and parameters

In order to process the H/V spectral ratios, several codes and methods were used. The classical H/V method was computed using the Geopsy <http://www.geopsy.org> software. It averages the ratio of the smoothed Fourier Transform of selected time windows. Tukey windows (cosine taper of 5% width) of 50 s long overlapping by 50% were selected. The smoothing was done using the Konno and Ohmachi [1998] procedure with a  $b$  value of 80. The classical method computed using the method of Fäh et al. [2001] was also performed

Moreover, the time-frequency analysis method [Fäh et al., 2009] was used to estimate the ellipticity function more accurately using the Matlab code of V. Poggi. In this method, the time-frequency analysis using the Wavelet transform is computed for each component. For each frequency, the maxima in time (10 per minute with at least 0.1 s between each) in the TFA are determined. The Horizontal to Vertical ratio of amplitudes for each maxima is then computed and statistical properties for each frequency are derived. The used wavelet is a Cosine wavelet with parameter 9. The mean of the distribution for each frequency is kept. For the sake of comparison, the time-frequency analysis by Fäh et al. [2001], based on the spectrogram, was also used, as well as the wavelet-based TFA coded in Geopsy.

The ellipticity extraction using the Capon analysis [Poggi and Fäh, 2010] (see section on array analysis) was also performed.

Method	Freq. band	Win. length	Anti-trig.	Overlap	Smoothing
Standard H/V Geopsy	0.5 – 20 Hz	50 s	No	50%	K&O 80
Standard H/V D. Fäh	0.5 – 20 Hz	30 s	No	75%	?
H/V TFA Geopsy	0.5 – 20 Hz	Morlet $m=8$ $fi=1$	No	-	?
H/V TFA D. Fäh	0.5 – 20 Hz	Specgram	No	-	?
H/V TFA V. Poggi	0.5 – 20 Hz	Cosine $wpar=9$	No	-	No

Table 4: Methods and parameters used for the H/V processing.

### 4.2 Results

Most of the H/V spectral ratios show approximately the same trend (Fig. 3) confirming the 1D assumption. However, in the classical approach, several peaks can be seen at 1.8, 2.3 and 4.1 Hz. At low frequencies, the H/V values are high and may be related to wind.

However, computing the HVTFA (Fig. 4) allows to remove a lot of complexity in the spectra that was maybe due to SH waves contribution. A clear peak around 4 Hz is now visible at all points except points VAM402 and VAM404. Using the Capon analysis (Fig. 5), the trend is similar but the amplitude are much lower and the peak insignificant. H/V ratios computed on a long-term recording at the current SVAM station (test station XVAM, Fig. 6), i.e. on a concrete slab in the transformer house, led to a characteristic peak at 3.8 Hz, that is however variable during the recording. Moreover, other peaks are observed between 2 and 3 Hz However Burjáněk et al. [2010] showed that the origin of the H/V peak may not be interpreted as the ellipticity of

Rayleigh waves in rock slopes. A polarization analysis of ambient vibration recordings at site SVAM was performed to confirm this. However, no clear polarization could be brought to light (high variability). Since this remains doubtful, the H/V information is not used in the inversion.

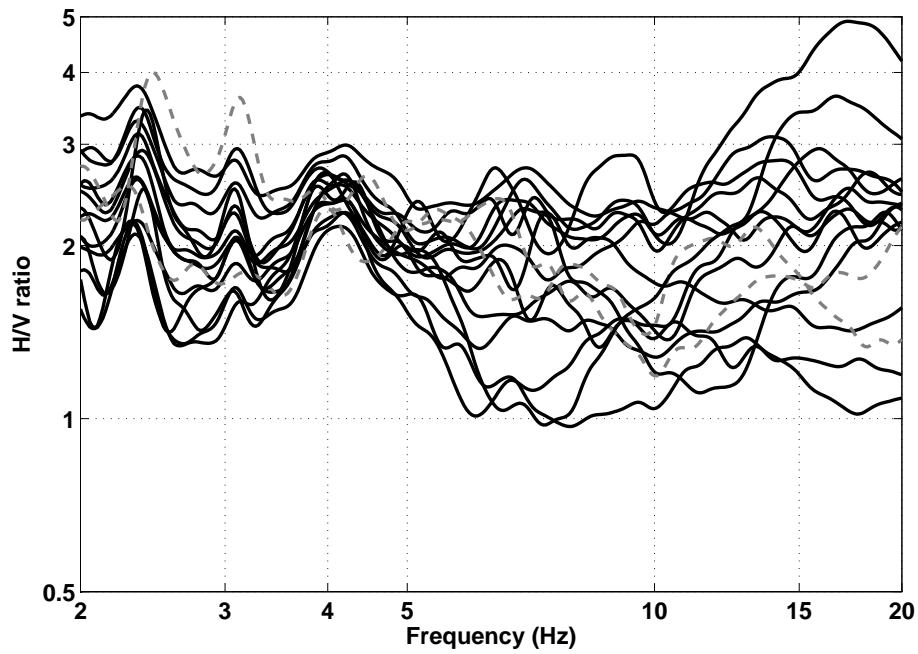


Figure 3: H/V spectral ratios of the array points using the classical method (Geopsy software). Points 402 and 404 are displayed in dashed grey lines.

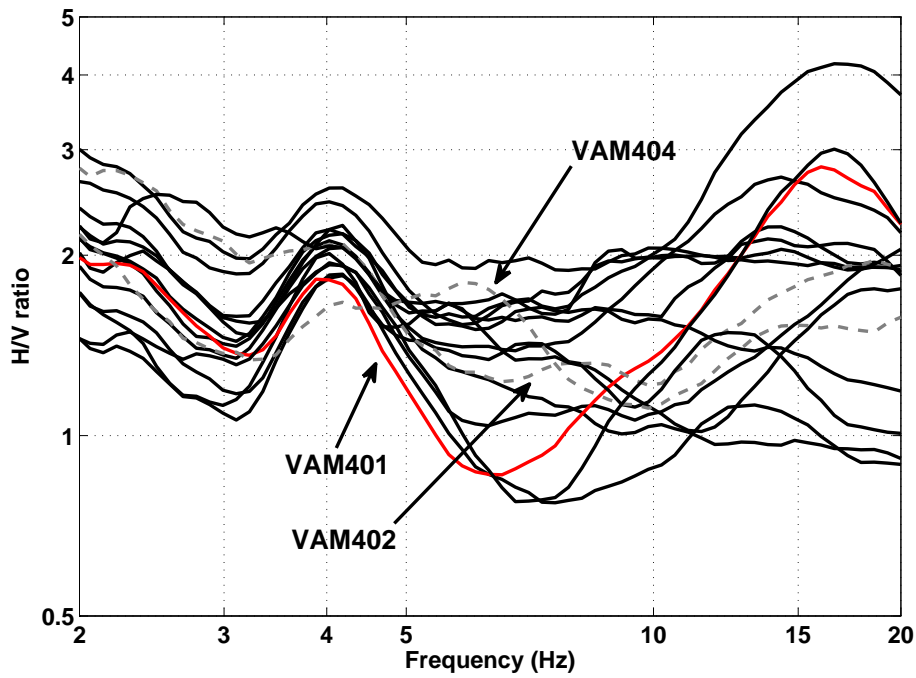


Figure 4: H/V spectral ratios of the array points using the time-frequency analysis method (V. Poggi's code). Points 402 and 404 provide different results, point 401 is the closest to station SVAM.

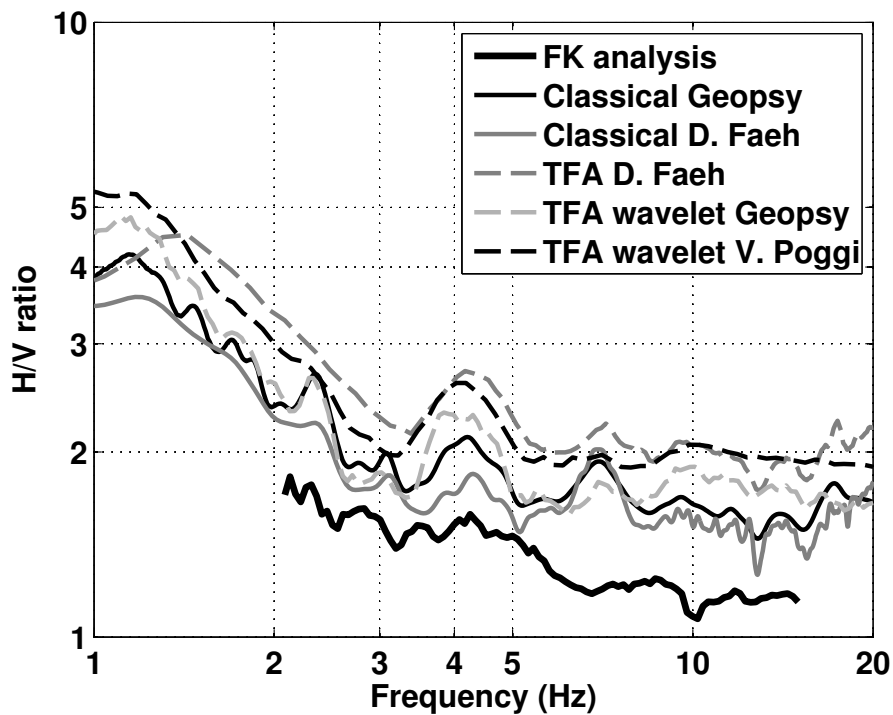


Figure 5: H/V spectral ratios for point VAM000 using the different codes. Classical methods were divided by  $\sqrt{2}$ .

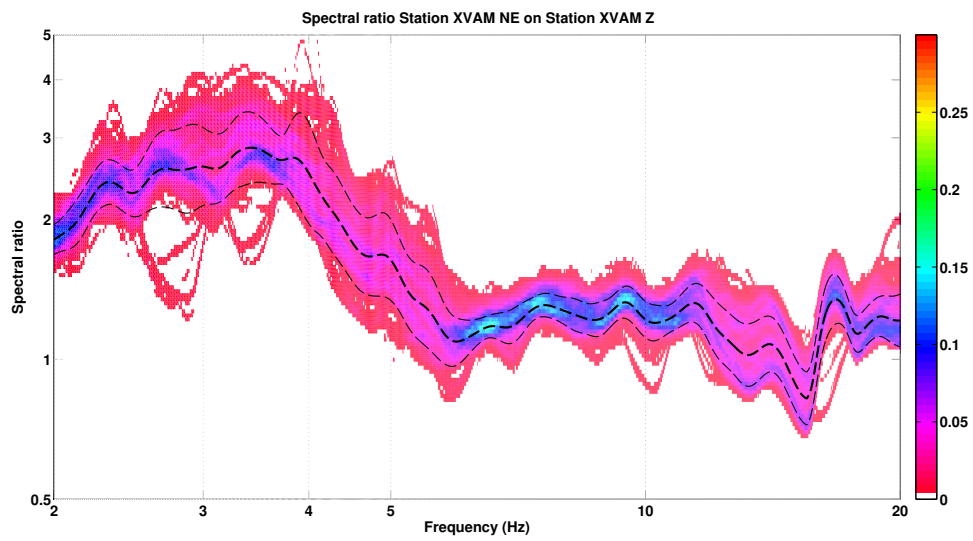


Figure 6: Distribution of H/V spectral ratios of the long-term station XVAM at site SVAM (values divided by  $\sqrt{2}$ ).

## 5 Array processing

### 5.1 Processing methods and parameters

The arrays were processed using the High-resolution FK analysis [Capon, 1969] using the Geopsy <http://www.geopsy.org> software.

Moreover, a 3C array analysis [Fäh et al., 2008] was also performed using the `array_tool_3C` software [Poggi and Fäh, 2010]. It allows to derive Rayleigh and Love modes. The results of computations of both datasets were assembled to estimate the dispersion curves.

Method	Dataset	Freq. band	Win. length	Anti-trig.	Overlap	Grid step	Grid size	# max.
HRFK 1C	1	2 – 15 Hz	500 <i>T</i>	No	50%	0.005	0.3	10
HRFK 1C	2	2 – 15 Hz	500 <i>T</i>	No	50%	0.005	0.3	10
HRFK 3C	1	2 – 15 Hz	Wav. 10 Tap. 0.2	No	50%	200 m/s	3000 m/s	5
HRFK 3C	2	2 – 15 Hz	Wav. 10 Tap. 0.2	No	50%	200 m/s	3000 m/s	5

Table 5: Methods and parameters used for the array processing.

### 5.2 Obtained dispersion curves

The first mode (Rayleigh) in the 1C FK analysis is picked between 3 and 13 Hz (Fig. 7) including its standard deviation. It shows a pronounced kink at 6 Hz. The velocities are high from 2500 m/s at 3 Hz down to 500 m/s at 13 Hz. A constant velocity of 330 m/s can be perfectly seen on the higher frequencies. It may be a sonic wave but its origin is unknown.

Using the 3C analysis, however, the interpretation of Rayleigh modes is different (Fig. 8). The kink is interpreted as an osculation point between the fundamental and the first higher mode. Therefore, the fundamental mode is picked in two chunks to avoid this critical part (Fig. 9). The radial component confirms this interpretation. The 330 m/s constant velocity is clear also on the vertical component, less on the radial and it does not appear on the transverse component. Transverse direction gives the fundamental Love mode from 3.5 to 8 Hz. The intermediate part is not clear and therefore not picked as well. The comparison between the 1C and 3C components highlights the interpretation difference, the inversion being performed with the 3C interpretation.

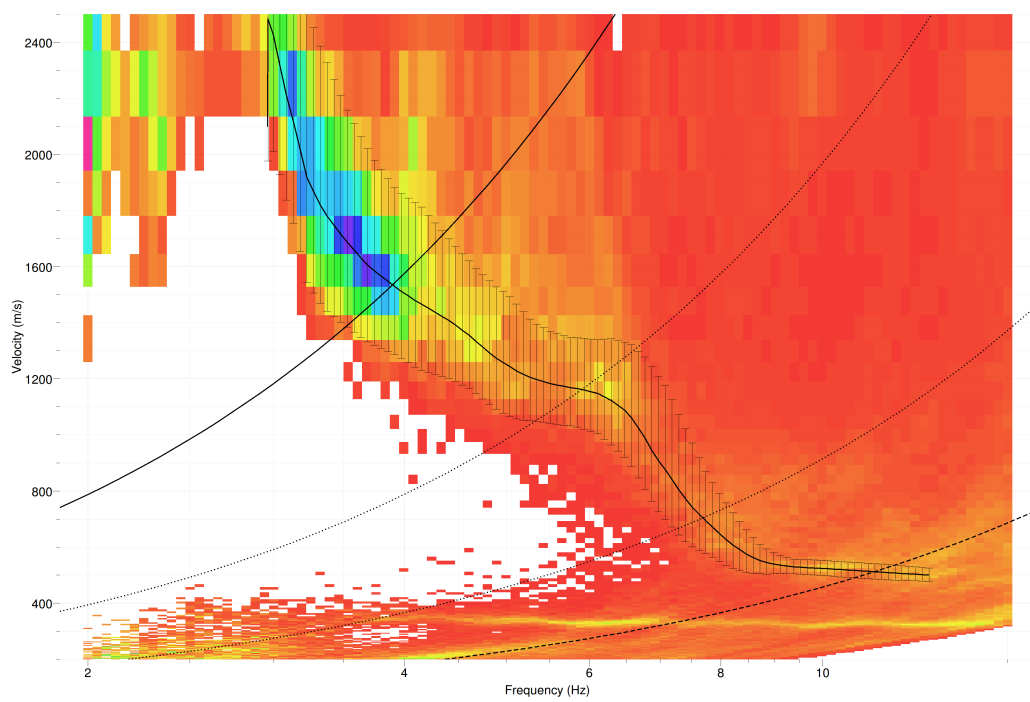


Figure 7: Dispersion curve obtained from the 1C array analysis.

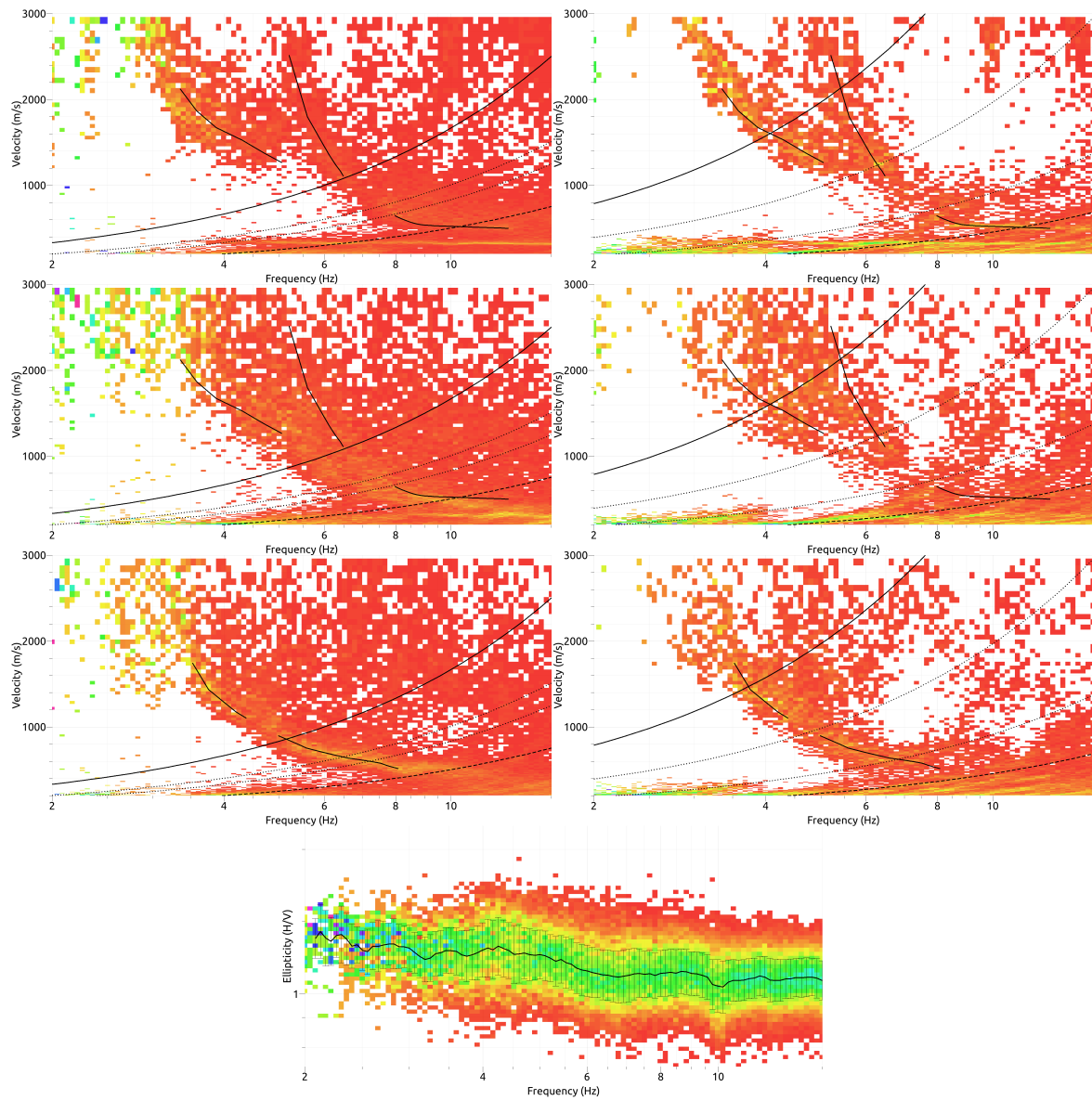


Figure 8: Dispersion curves obtained from the 3C array analysis. From top to bottom: Vertical, radial and transverse components. Left: first dataset; Right: second dataset. Bottom: ellipticity from both datasets.

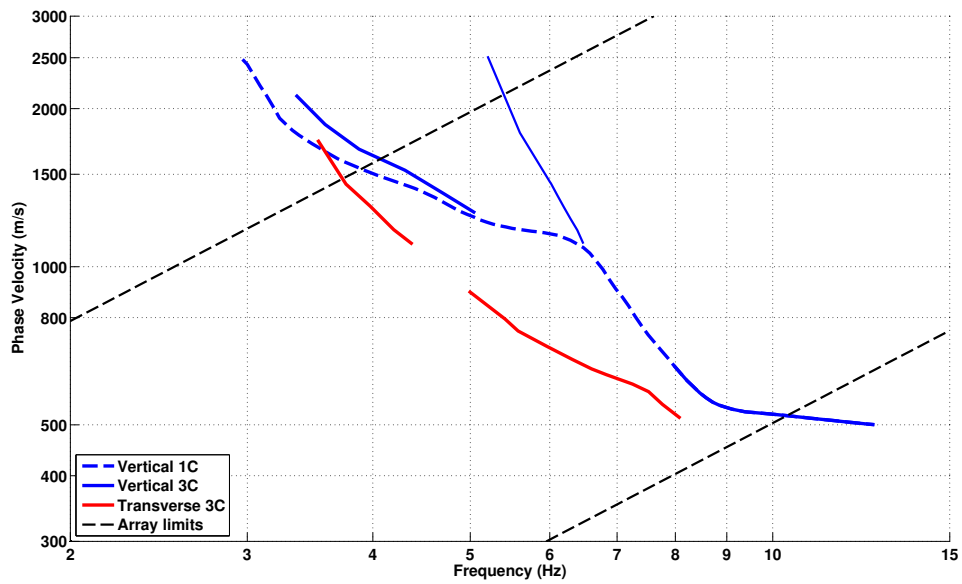


Figure 9: Comparison of obtained dispersion curves using 1C and 3C analyses.

## 6 Inversion and interpretation

### 6.1 Inversion

For the inversion, the Love and the Rayleigh fundamental modes (3C analysis) and the Rayleigh first higher mode dispersion curves without standard deviation to avoid different weighting were used as simultaneous targets. Attempts using the interpretation of the 1C analysis failed. All curves were resampled using 50 points between 2 and 15 Hz in log scale.

The inversion was performed using the Improved Neighborhood Algorithm (NA) Wathelet [2008] implemented in the Dinver software. In this algorithm, the tuning parameters are the following:  $N_{s_0}$  is the number of starting models, randomly distributed in the parameter space,  $N_r$  is the the number of best cells considered around these  $N_{s_0}$  models,  $N_s$  is the number of new cells generated in the neighborhood of the  $N_r$  cells ( $N_s/N_r$  per cell) and  $It_{max}$  is the number of iteration of this process. The process ends with  $N_{s_0} + N_r * \frac{N_s}{N_r} * It_{max}$  models. The used parameters are detailed in Tab. 6.

$It_{max}$	$N_{s_0}$	$N_s$	$N_r$
500	10000	100	100

Table 6: Tuning parameters of Neighborhood Algorithm.

During the inversion process, low velocity zones were not allowed. The Poisson ratio was supposed uniform in each layer in the range 0.2-0.4 and the density was supposed equal to  $2000 \text{ kg/m}^3$  in the sediments and  $2500 \text{ kg/m}^3$  in the lowest layer. 2 layers over a half-space are enough to explain the targets (dispersion curves), but more layers are then used to smooth the obtained results and better explore the parameter space. Fixed depth layers parametrization were also included. 5 independent runs of 5 different parametrization schemes (3, 4 and 5 layers over a half space and 12 and 14 fixed depth layers) were performed. For further elaborations, the best models of these 25 runs were selected (Fig. 12).

The retrieved velocity profiles exhibit a first layer of about 5 m depth with low velocities (200 m/s). At this depth a clear interface is found with a lower layer with velocities around 700 m/s . Finally, the bedrock is found at 45 m depth with a velocity around 2700 m/s, not really constrained, though.

When comparing to the target curves (Fig. 10 and Fig. 11), all dispersion curves are perfectly represented, so that no more detailed profiles can be retrieved from these data. The ellipticity peak is also found at the right frequency but with much higher amplitudes, though.

The inverted model represents the first meters of sand (according to the geological map) with low cohesion possibly followed by weathered rock down to the bedrock.

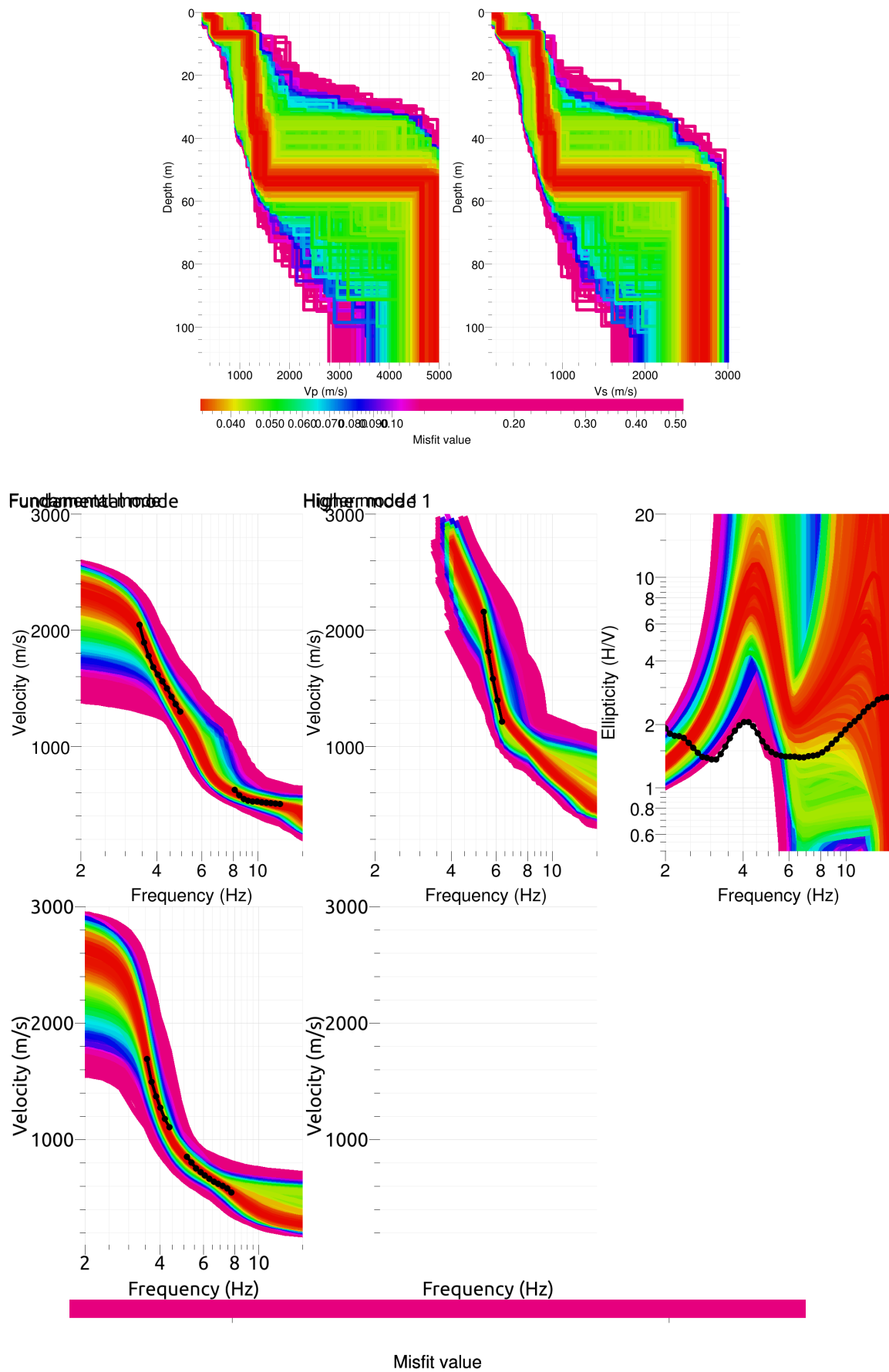


Figure 10: Inverted ground profiles in terms of  $V_p$  and  $V_s$  (top) and comparison between inverted models and measured Rayleigh and Love modes and corresponding ellipticity, free layer depth strategy.

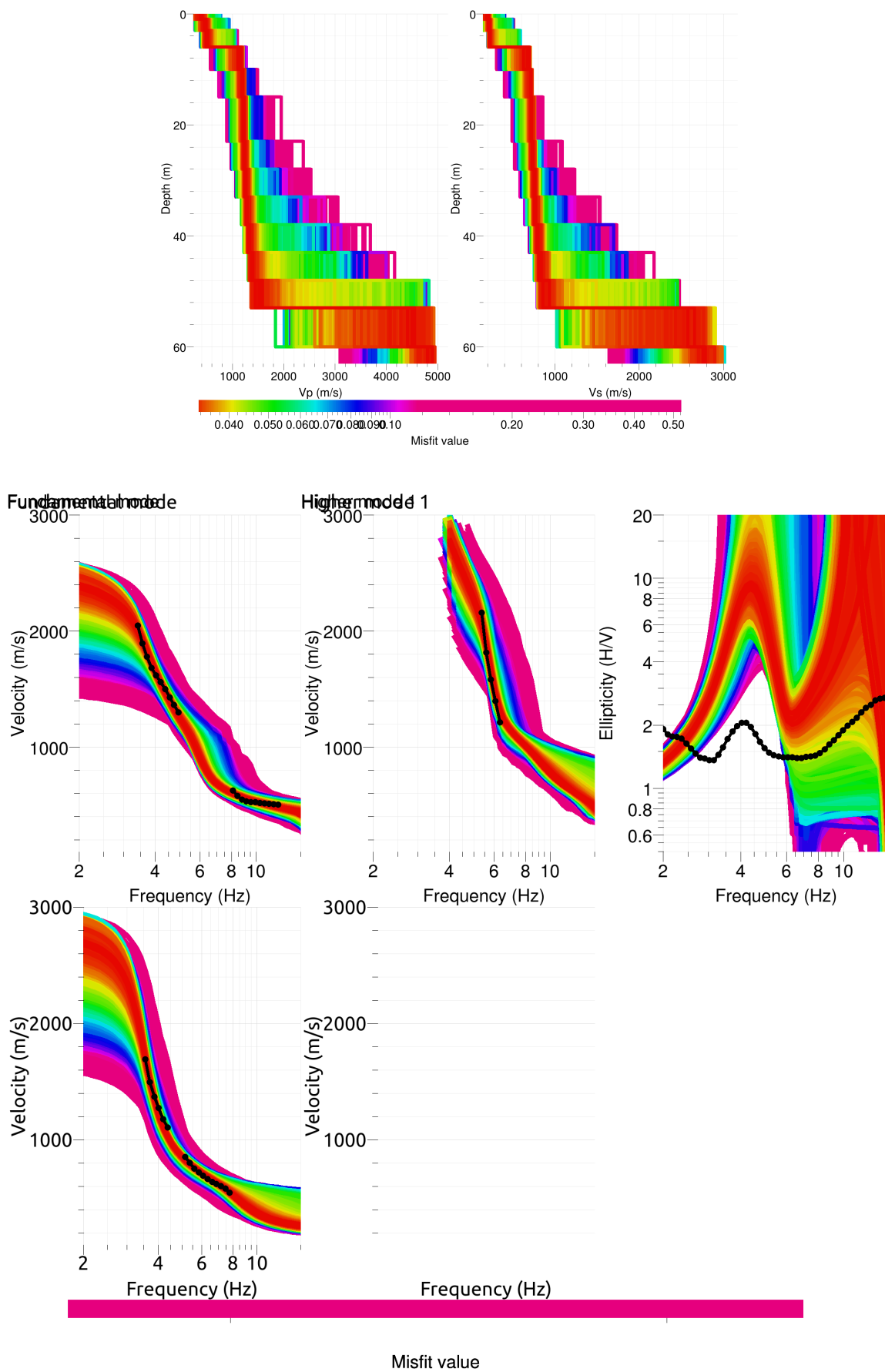


Figure 11: Inverted ground profiles in terms of  $V_p$  and  $V_s$  (top) and comparison between inverted models and measured Rayleigh and Love modes and corresponding ellipticity, fixed layer depth strategy.

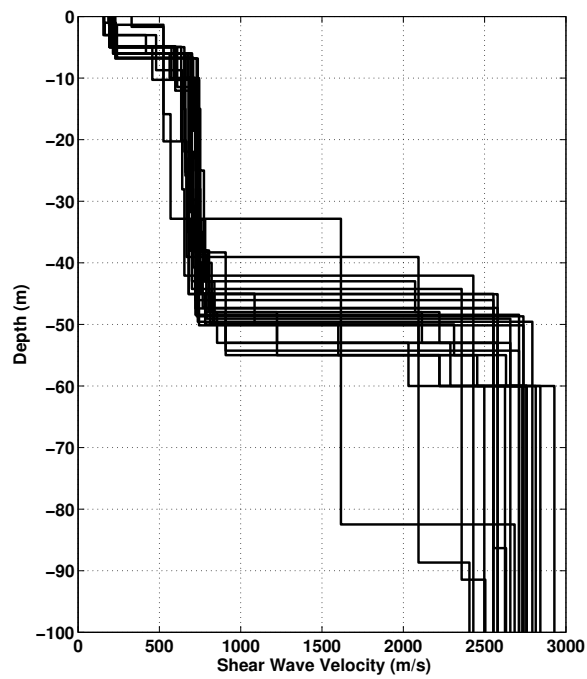


Figure 12:  $V_s$  ground profiles for the selected 25 best models.

## 6.2 Travel time average velocities and ground type

The distribution of the travel time average velocities at different depths was computed from the selected models. The uncertainty, computed as the standard deviation of the distribution of travel time average velocities for the considered models, is also provided, but its meaning is doubtful.  $V_{s,30}$  is found to be 486 m/s, which corresponds to class B in the Eurocode 8 [CEN, 2004]. For SIA261 [SIA, 2003], the first 5 m at low velocity on weathered rock at about 700 m/s make this site fall in ground type E. This is not the case for EC8 because the lowest layer has a velocity lower than 800 m/s.

	Mean (m/s)	Uncertainty (m/s)
$V_{s,5}$	226	57
$V_{s,10}$	310	46
$V_{s,20}$	422	22
$V_{s,30}$	486	16
$V_{s,40}$	531	19
$V_{s,50}$	582	29
$V_{s,100}$	-	-
$V_{s,150}$	-	-
$V_{s,200}$	-	-

Table 7: Travel time averages at different depths from the inverted models. Uncertainty is given as one standard deviation from the selected profiles.

## 6.3 SH transfer function and quarter-wavelength velocity

The quarter-wavelength velocity approach [Joyner et al., 1981] provides, for a given frequency, the average velocity at a depth corresponding to 1/4 of the wavelength of interest. It is useful to identify the frequency limits of the experimental data (minimum frequency in dispersion curves at 3.4 Hz here). The results using this proxy show that the dispersion curves constrain the profiles down to 40 m (Fig. 13). Moreover, the quarter wavelength impedance-contrast introduced by Poggi et al. [2012] is also displayed in the figure. It corresponds to the ratio between two quarter-wavelength average velocities, respectively from the top and the bottom part of the velocity profile, at a given frequency [Poggi et al., 2012]. It shows a trough (inverse shows a peak) at the resonance frequency.

Moreover, the theoretical SH-wave transfer function for vertical propagation [Roesset, 1970] is computed from the inverted profiles. It is compared to the quarter-wavelength amplification [Joyner et al., 1981] that however cannot take resonances into account (Fig. 14). In this case, the models are predicting large amplifications especially at 3.8 and 9 Hz.

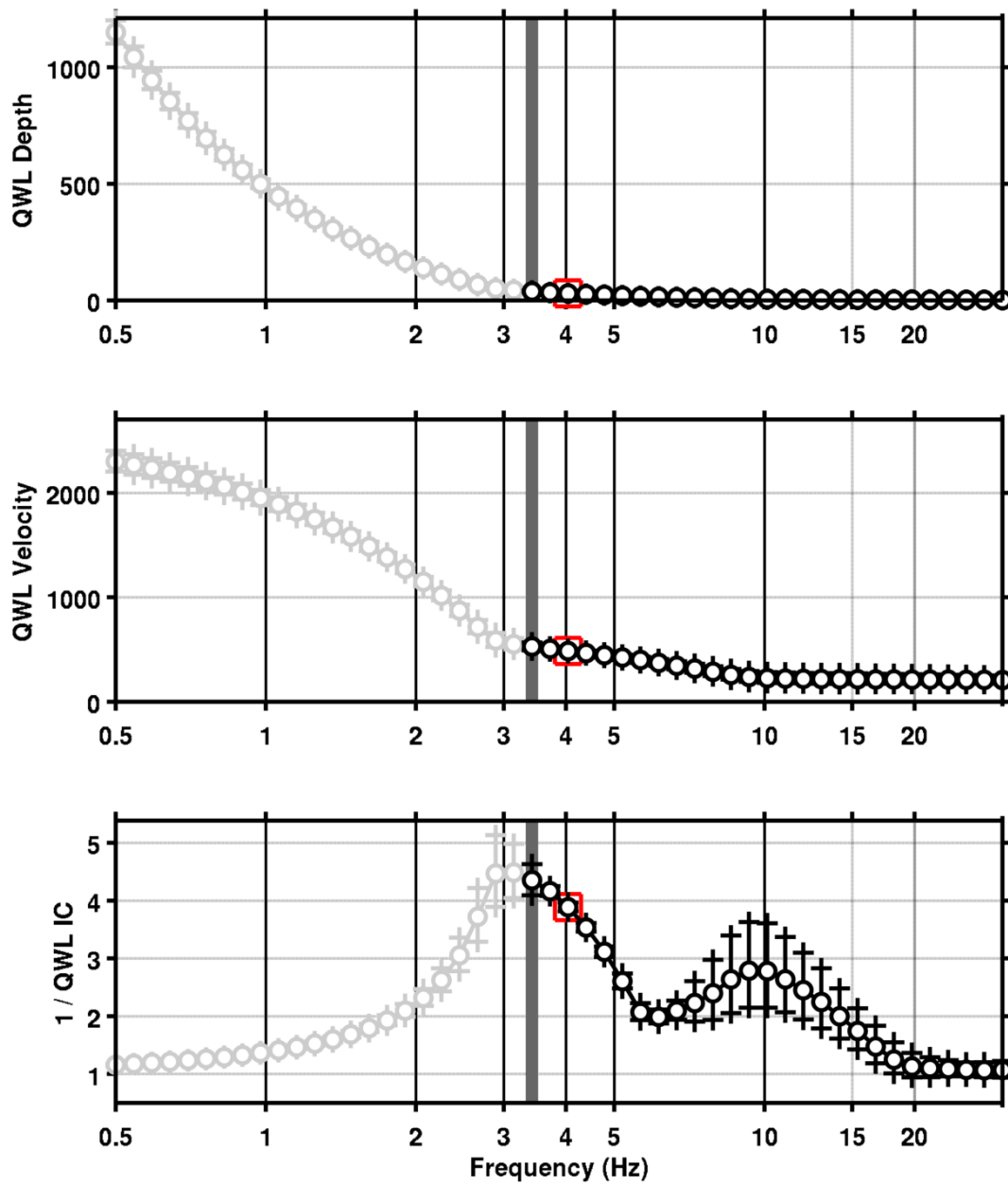


Figure 13: Quarter wavelength velocity representation of the velocity profile (top: depth, centre: velocity, bottom: inverse of the impedance contrast). Black curve is constrained by the dispersion curves, light grey is not constrained by the data. Red square is corresponding to  $V_{s,30}$ .

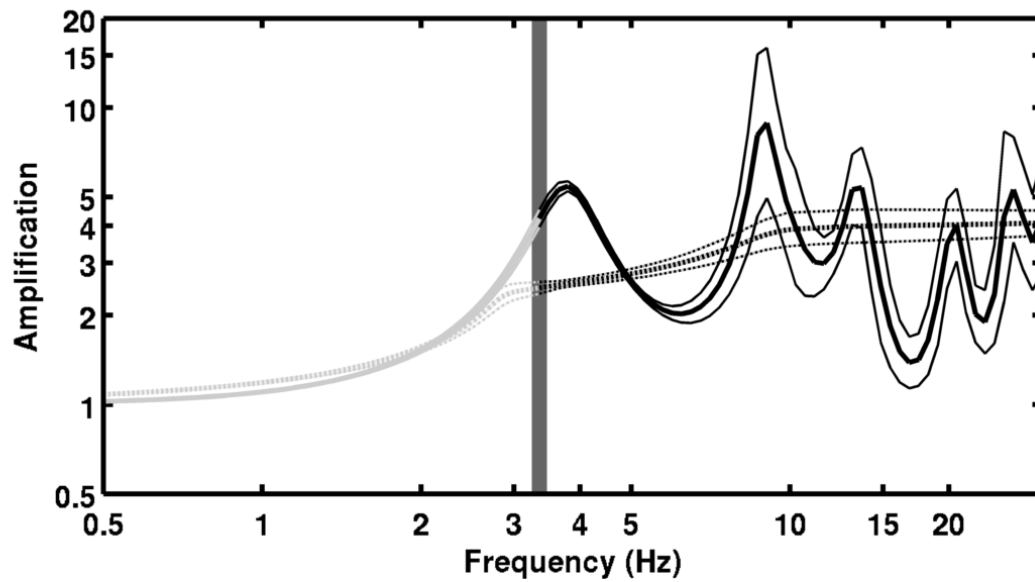


Figure 14: Theoretical SH transfer function (solid line) and quarter wavelength impedance contrast (dashed line) with their standard deviation. Significance of the greyscale is detailed in Fig. 13.

## 7 Conclusions

Ambient vibration arrays in Obervaz could provide information on the site down to about 50 m. The H/V peak in the array points was however found to be stable in the array but variable in time, around 4 Hz. This might be due to the fractured rock in the moving rock-slope [Burjáněk et al., 2010].

The retrieved velocity profiles exhibit a 5 m depth layer of sand (200 m/s) and a layer of weathered rock (700 m/s) down to the bedrock at 45 m depth with a velocity around 2700 m/s (not really constrained).  $V_{s,30}$  is found to be 486 m/s. The site can be classified as type B in the Eurocode 8 and type E in the Swiss Code SIA261. Other geological and geophysical data should be collected to learn more about this mass movement, the distribution of the sand layer and the weathering and fracturing of the rock. Recordings at the station will also allow to update the assumptions made here.

## Acknowledgements

The authors thank Marko Terzic for the help during these measurements.

## References

- Sylvette Bonnefoy-Claudet, Fabrice Cotton, and Pierre-Yves Bard. The nature of noise wavefield and its applications for site effects studies. *Earth-Science Reviews*, 79(3-4): 205–227, December 2006. ISSN 00128252. doi: 10.1016/j.earscirev.2006.07.004. URL <http://linkinghub.elsevier.com/retrieve/pii/S0012825206001012>.
- Jan Burjánek, Gabriela Gassner-Stamm, Valerio Poggi, Jeffrey R. Moore, and Donat Fäh. Ambient vibration analysis of an unstable mountain slope. *Geophysical Journal International*, 180(2):820–828, February 2010. ISSN 0956540X. doi: 10.1111/j.1365-246X.2009.04451.x. URL <http://doi.wiley.com/10.1111/j.1365-246X.2009.04451.x>.
- J. Capon. High-Resolution Frequency-Wavenumber Spectrum Analysis. *Proceedings of the IEEE*, 57(8):1408–1418, 1969.
- CEN. *Eurocode 8: Design of structures for earthquake resistance - Part 1: General rules, seismic actions and rules for buildings*. European Committee for Standardization, en 1998-1: edition, 2004.
- Donat Fäh, Fortunat Kind, and Domenico Giardini. A theoretical investigation of average H / V ratios. *Geophysical Journal International*, 145:535–549, 2001.
- Donat Fäh, Gabriela Stamm, and Hans-Balder Havenith. Analysis of three-component ambient vibration array measurements. *Geophysical Journal International*, 172(1):199–213, January 2008. ISSN 0956540X. doi: 10.1111/j.1365-246X.2007.03625.x. URL <http://doi.wiley.com/10.1111/j.1365-246X.2007.03625.x>.
- Donat Fäh, Marc Wathelet, Miriam Kristekova, Hans-Balder Havenith, Brigitte Endrun, Gabriela Stamm, Valerio Poggi, Jan Burjanek, and Cécile Cornou. Using Ellipticity Information for Site Characterisation Using Ellipticity Information for Site Characterisation. Technical report, NERIES JRA4 Task B2, 2009.
- William B. Joyner, Richard E. Warrick, and Thomas E. Fumal. The effect of Quaternary alluvium on strong ground motion in the Coyote Lake, California, earthquake of 1979. *Bulletin of the Seismological Society of America*, 71(4):1333–1349, 1981.
- Katsuaki Konno and Tatsuo Ohmachi. Ground-Motion Characteristics Estimated from Spectral Ratio between Horizontal and Vertical Components of Microtremor. *Bulletin of the Seismological Society of America*, 88(1):228–241, 1998.
- Valerio Poggi and Donat Fäh. Estimating Rayleigh wave particle motion from three-component array analysis of ambient vibrations. *Geophysical Journal International*, 180(1):251–267, January 2010. ISSN 0956540X. doi: 10.1111/j.1365-246X.2009.04402.x. URL <http://doi.wiley.com/10.1111/j.1365-246X.2009.04402.x>.
- Valerio Poggi, Benjamin Edwards, and D. Fah. Characterizing the Vertical-to-Horizontal Ratio of Ground Motion at Soft-Sediment Sites. *Bulletin of the Seismological Society of America*, 102(6):2741–2756, December 2012. ISSN 0037-1106. doi: 10.1785/0120120039. URL <http://www.bssaonline.org/cgi/doi/10.1785/0120120039>.

- J.M. Roesset. Fundamentals of soil amplification. In R. J. Hansen, editor, *Seismic Design for Nuclear Power Plants*, pages 183–244. M.I.T. Press, Cambridge, Mass., 1970. ISBN 978-0-262-08041-5. URL <http://mitpress.mit.edu/catalog/item/default.asp?ttype=2&tid=5998>.
- SIA. *SIA 261 Actions sur les structures porteuses*. Société suisse des ingénieurs et des architectes, Zürich, sia 261:20 edition, 2003.
- Marc Wathélet. An improved neighborhood algorithm: Parameter conditions and dynamic scaling. *Geophysical Research Letters*, 35(9):1–5, May 2008. ISSN 0094-8276. doi: 10.1029/2008GL033256. URL <http://www.agu.org/pubs/crossref/2008/2008GL033256.shtml>.